

**In-line monitoring of the fused filament fabrication additive manufacturing process for short fibre-reinforced composites.**

FORSTER, Rosanna, FETEIRA, Antonio <<http://orcid.org/0000-0001-8151-7009>>, SOULIOTI, Dimitra, GRAMMATIKOS, Sotirios and KORDATOS, Evangelos <<http://orcid.org/0000-0002-5448-3883>>

Available from Sheffield Hallam University Research Archive (SHURA) at:

<https://shura.shu.ac.uk/35624/>

---

This document is the Accepted Version [AM]

**Citation:**

FORSTER, Rosanna, FETEIRA, Antonio, SOULIOTI, Dimitra, GRAMMATIKOS, Sotirios and KORDATOS, Evangelos (2025). In-line monitoring of the fused filament fabrication additive manufacturing process for short fibre-reinforced composites. In: FERRARINI, Giovanni, SPAETH, Peter and LÓPEZ, Fernando, (eds.) SPIE Proceedings Volume 13047, Thermosense: Thermal Infrared Applications XLVII. SPIE. [Book Section]

---

**Copyright and re-use policy**

See <http://shura.shu.ac.uk/information.html>

# **In-line monitoring of the fused filament fabrication additive manufacturing process for short fibre-reinforced composites.**

**Authors:** R. Forster<sup>\*a</sup> A. Feteira<sup>a</sup> D. Soulioti<sup>a</sup> S. Grammatikos<sup>b</sup>, E. Kordatos<sup>\*a</sup>

<sup>a</sup>School of Engineering and Built Environment, Howard Street, Sheffield Hallam University, Sheffield S1 1WB, UK

<sup>b</sup>ASEMLab – Laboratory of Advanced and Sustainable Engineering Materials, Department of Manufacturing and Civil Engineering, Norwegian University of Science and Technology, Gjøvik, 2815, Norway

## **ABSTRACT**

In the present work, a combination method of acoustic emission (AE) and infrared thermography (IR) alongside micro-computed tomography has been developed for the detection and monitoring of defects in additively manufactured fibre-reinforced polymer matrix composites. This method allows for the detection of anomalies and defects during the printing process and the verification of their presence in the finished printed structure without the need for destructive testing. Furthermore, a structural assessment of these materials was performed with tensile testing alongside IR monitoring. For both the in-line monitoring and the structural assessment, the correlation between the printing parameters, the presence of defects and anomalies and the mechanical properties was investigated.

**Keywords:** Fibre-reinforced composites, Acoustic Emission, Infrared Thermography, Tensile Testing, additive manufacturing, Non-destructive Evaluation, 3d printing, polymer matrix composites.

[\\*R.Forster@shu.ac.uk](mailto:R.Forster@shu.ac.uk), [E.Kordatos@shu.ac.uk](mailto:E.Kordatos@shu.ac.uk)

## **1. INTRODUCTION**

Additive Manufacturing (AM) is a rapidly growing area of technology for the creation of polymer matrix composites due to the geometric flexibility, lack of post-processing required, and minimal waste produced [1] [2]. The technology works by creating a physical 3D model based on a part produced through computer-aided design (CAD) [3]. Fused Filament Fabrication (FFF) is an extrusion based AM method and is the most commonly used technique to produce fibre-reinforced polymer matrix composites (FRPs), which have a wide range of applications including aerospace, automotive, biomedical and R&D [1]. Composite materials generally have superior properties than conventional materials including specific properties at a reduced weight and stiffness [4], however those manufactured through traditional methodologies are limited though the need for post-production material removal, high cost and high wastage.

FFF is a layer based process, where filament material is heated and extruded in a semi-molten state through a nozzle onto a print bed which then solidifies and hardens. The next layer is then extruded on top and solidifies to the previous layer, fusing together. This process is repeated until the desired print shape is created [5]. It is widely reported that printing parameters such as layer height [6], print temperature, print speed and printing orientation have a significant effect on the quality and mechanical properties of the printed parts [7] [8].

The nature of the printing process allows for the creation of defects such as porosity, voids and cracks [9]. Detection of these at the time of printing is difficult as once the printing process has begun, if interrupted, it will have to be abandoned and restarted on most printers. The technology to detect these errors is not consistently reliable and, whilst able to identify missing layers and excess vibration, cannot detect smaller defects such as intra-layer porosity. Short-fibre reinforced composites (SFRPs) are also susceptible to defects such as nozzle clogging and poor fibre/ matrix interface bonding created by the introduction of fibres into the filament material.

One method of detection of these issues during the printing process is the application of non-destructive evaluation (NDE) techniques. Although applying NDE to composite materials has been proven challenging [9], Infrared Thermography (IR) [10] and Acoustic emission (AE) [11] and Micro-computed Tomography (Micro-CT) [12] have all found success in detecting defects in FRP FFF parts. IR allows for the detection of uneven material deposition, retained heat monitoring and unexpected material cooling behaviours. AE can detect unexpected acoustic events which can provide indicators of defect or anomaly formation.

In the present work, we present a combination method of AE and IR has been developed for the detection and monitoring of defects in AM FRPs. This method of in-line monitoring will be supported by the results of offline assessment through Micro-CT to benchmark the findings. A structural assessment of the materials was performed with tensile testing alongside IR monitoring and for both the in-line monitoring and the structural assessment, the correlation between the printing parameters, the presence of defects and anomalies and the mechanical properties was investigated.

## **2. EXPERIMENTAL SETUP**

### **2.1 Printing**

Printing of the short-fibre reinforced polymer samples was performed on an Anisoprint Desktop Composer A3 printer, through the plastic nozzle with a nozzle diameter of 0.4mm. The cubed samples printed were 10mm<sup>3</sup> with a 5 loop brim and skirt to aid adhesion and material deposition alongside Magigoo PA adhesive glue. The tensile test samples were BS EN ISO 527-4:2023 qualification Type 1B [13] and printed in sets of 3.

The filament of the short-fibre reinforced filament was Smooth PA with a filament diameter of 1.75mm [14]. Smooth PA is a pre-impregnated PA12 filament reinforced with 10% dispersed carbon fibre and the material profile provided in AURA was used for the printing settings. The macrolayer height was changed to allow for the determination of the effect of changing the printing parameters. The printing profiles as well as some of the key parameters are listed in Table 1. Adhering to the datasheets for this material, the samples were annealed before structural assessment [14]. The samples were annealed at 100°C for 6 hours and were allowed to slow cool and then stored in an airtight bag containing SilicaGel Desiccant packets to reduce moisture.

Table 1 - Smooth PA printing profile parameters.

	0.1mm Macrolayer	0.15mm Macrolayer	0.2mm Macrolayer	0.3mm Macrolayer	1mm Macrolayer
Macro Layer Height (mm)	0.1	0.15	0.2	0.3	1
External Shell Layer Height (mm)	0.05	0.075	0.1	0.15	0.5
Plastic Perimeters Layer Height (mm)	0.05	0.075	0.1	0.15	0.5
Infill Layer Height (mm)	0.1	0.15	0.2	0.3	1
Thick support layer height (mm)	0.1	0.15	0.2	0.3	1
Infill Density (%)	100	100	100	100	100
First Layer Height (mm)	0.25	0.25	0.25	0.25	0.25
Cube Print Time (mins)	57	39	29	19	6

## 2.2 In-line Monitoring

The experimental setup for the printing process can be seen in Figure 1. The IR results were recorded with a FLIR X6540sc camera [15] with a cooled Indium antimonide (InSb) detector. The capturing frame rate was 101.0Hz with a range of 5-300.0°C, and a field of view (FOV) of 11°x8.8°. The sensitivity was of >25mK. The camera was connected to a laptop which was recording the output data through FLIR IR software.

The AE data was collected with MISTRAS Micro-II express digital AE equipment, with a 20db gain pre-amplifier (2/4/6) to enhance the AE signals. A wideband AE sensor with a frequency range of 100-900kHz [16] was attached to the print head of the Composer A3 with tape as seen in Figure 1 with ANAGEL ultrasound gel applied to aid in the acoustic coupling. The data was processed in AEWIn software.

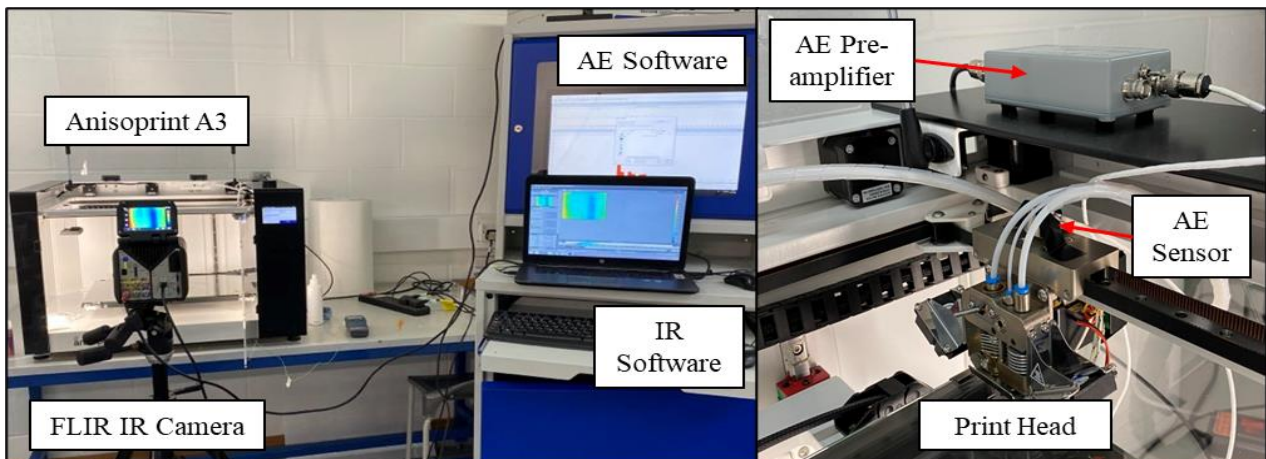


Figure 1 - Printing and in-line monitoring setup.

### 2.3 Offline Assessment

Micro-CT was performed on a Bruker Skyscan 1272 equipment [17]. It was used to analyse the internal structure of the printed cubes by loading them onto a raised surface, fixed in place with dental wax and rotated, with images being taken at a set rotation step layer by layer.

The filter applied was  $AL = 0.25\text{mm}$  with an elevation of  $12\text{mm}$ . The test selected was a source current of  $200\mu\text{A}$  and a source voltage of  $45\text{kV}$ . The pixel resolution was  $10\mu\text{m}$  with averaging frames of 3 and a  $0.7^\circ$  rotation step. The samples were scanned about  $180^\circ$  with a  $2016 \times 1344$  camera. Once scanning was finished, the images are loaded into NRecon using GPUReconServer where any scanning artifacts such as circle artifacts are removed, and smoothing is performed. The images were then aligned using DataViewer, rendered as a volume render in CTVox and analyses in CTAn where they underwent custom post-processing to allow for porosity percentage measurements.

### 2.4 Structural Assessment

Tensile testing was carried out on an Instron Universal Testing machine (Model 3369) with a Digital Extensometer AVE2, with the setup displayed in Figure 2. Tests were conducted in accordance with BS EN ISO 527-4:2023 qualification Type 1B test standard. The IR results were recorded with a FLIR X6540sc camera with a cooled Indium antimonide (InSb) detector. The camera was connected to a laptop which was recording the output data through FLIR IR software.

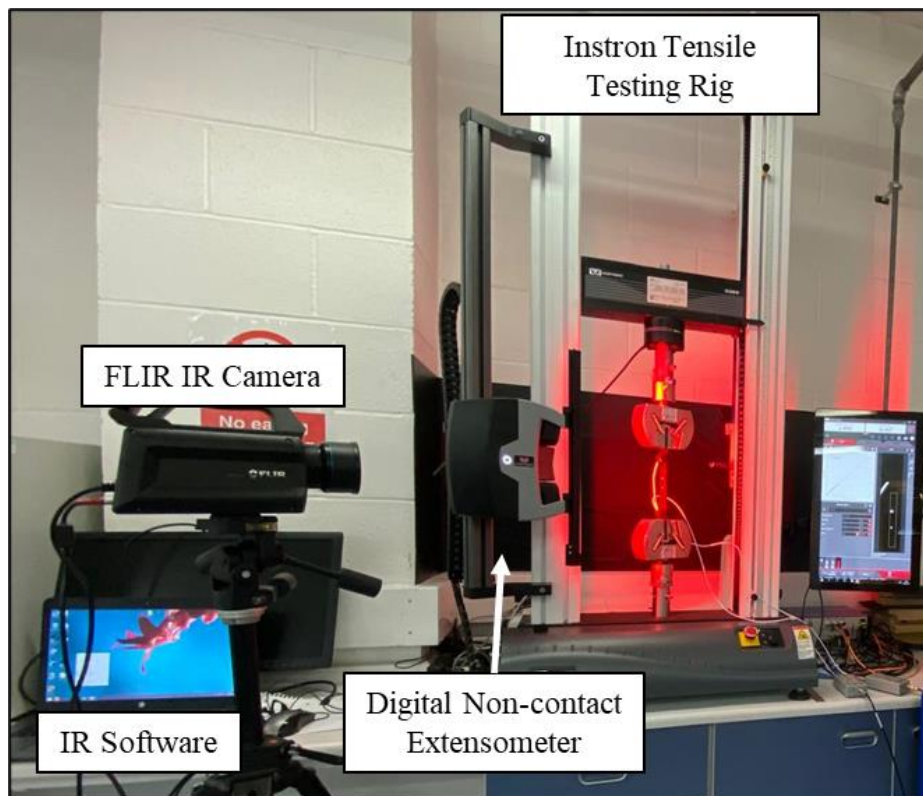


Figure 2 - Tensile testing equipment setup with IR monitoring

### 3. RESULTS

#### 3.1 In-Line Monitoring

##### 3.1.1 IR

Figure 3 shows the IR thermographs and temperature profiles during the printing process with the profile results presented graphically. Expected thermal behaviours for these samples would show a lower temperature to the left of the image and a hotter, more red material to the right of the image. Variation from this distribution could indicate poor cooling and poor bonding as the correct material temperature is highly important to ensure layer adhesion and minimal porosity. The 0.3mm cube shows clear variation from the expected distribution with a peak to the left of the plot. From the thermograph, it is clear that there is uneven thermal distribution, with more material deposited on the left side of the sample. This can be an indicator for the creation of a defect as this extra material hasn't cooled in the expected way and can lead to the formation of voids. The 1mm sample also shows a clear and more drastic deviation from the expected thermal distribution. The sample is not cooling as expected, with multiple peaks along the print path across a 12°C range when compared to the 0.1mm sample, which has a fairly consistent cooling curve over a range of 35°C.

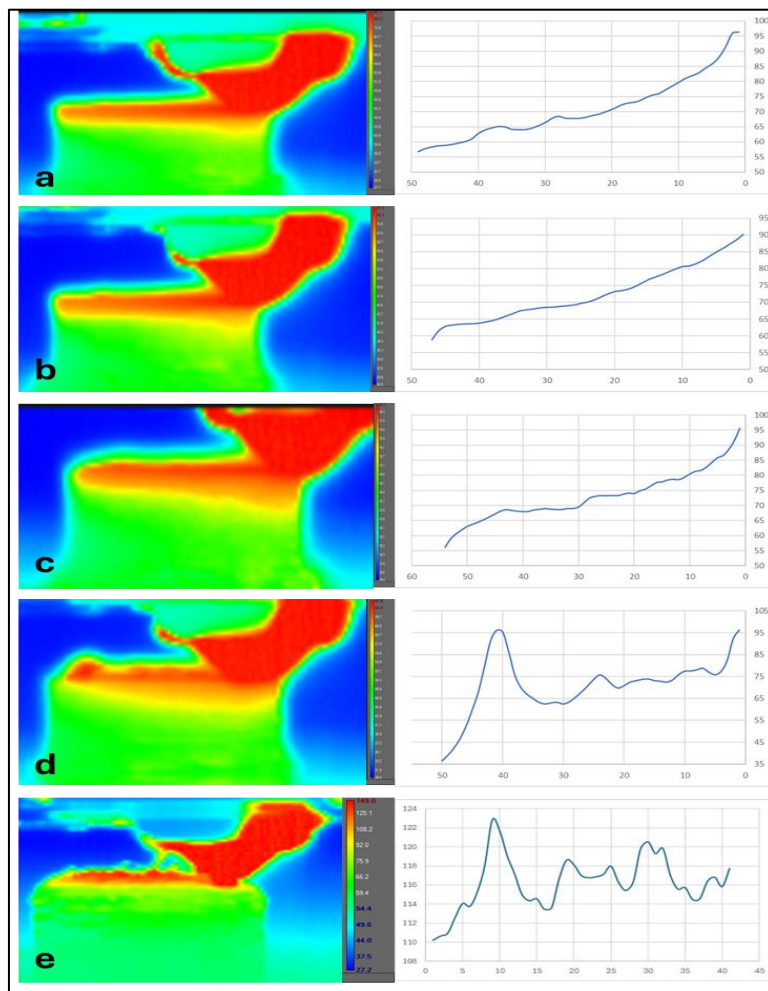


Figure 3 - IR thermographs and pixel plots for all samples, a) 0.1mm, b) 0.15mm, c) 0.2mm, d) 0.3mm and e) 1mm.

This is a clear indicator for poor layer adhesion incorrect cooling and could also have an effect on the retained heat within the sample. There is a clear trend as the macrolayer height increases, the uneven thermal distribution increases and as such, increased indicators of defects.

### 3.1.2 AE

Figure 4 presents the AE results. Due to the nature of the printing process, there will be regular repeated acoustic events as the print head follows its path as well as equipment and fan vibration. A threshold of 30db was applied to account for the background noise. Initial results of hits across the print time were recorded and normalised for the print time and number of layers within the sample. A higher number of these normalised hits indicate the presence of more defects as regular movement is accounted for by thresholding.

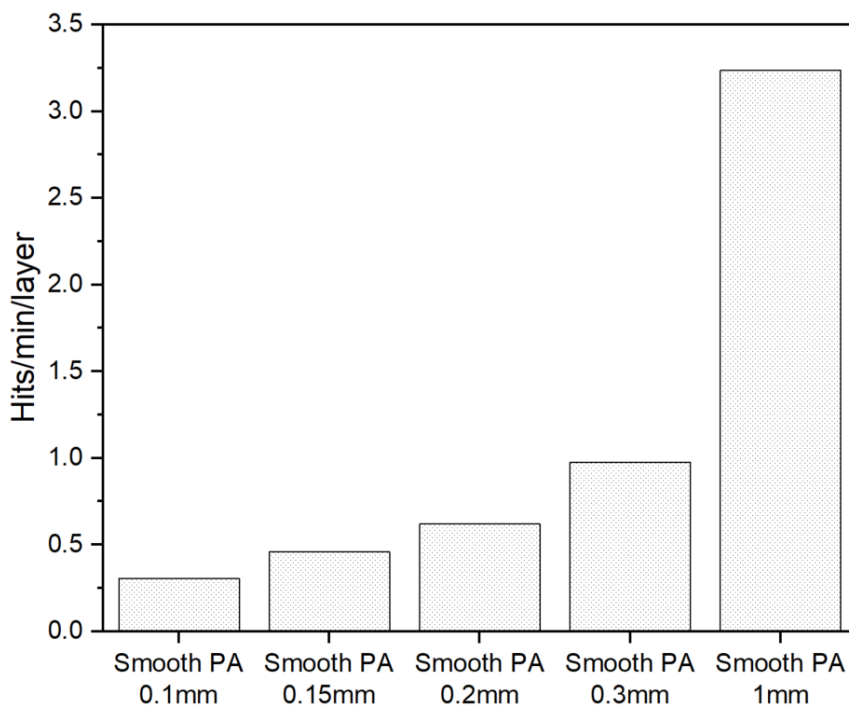


Figure 4 - Comparison of normalised hits across all profiles.

Following the trend seen within the IR monitoring, as the macrolayer height increases, the number of indicators of defects increase. The 0.1mm sample with the longest print time and the greatest number of layers showed the least number of normalised hits, with less unexpected acoustic events and indicators of defects. The number of normalised hits increased as the print time decreased, showing an inverse relationship with the 1mm sample recording a 952% increase compared to the 0.1mm sample.

### 3.2 Offline Assessment

Figure 5 shows the CTVox renderings of the cubed samples, with an image slice taken from within the infill of the cubes. The grey material represents the composite material, and the darker area represent a less dense material, which in this case indicates air and therefore voids and porosity.

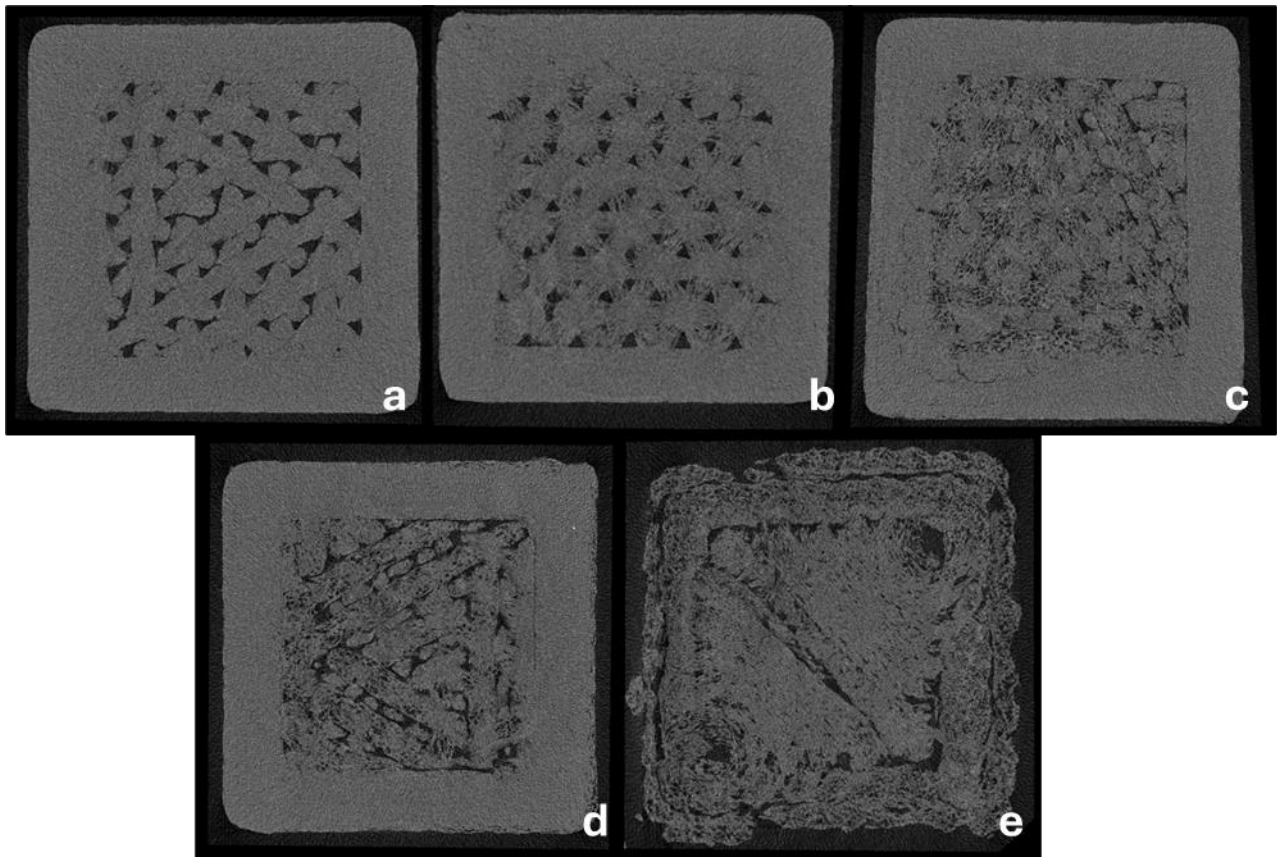


Figure 5 - CTVox renderings of all samples a) 0.1mm, b) 0.15mm, c) 0.2mm, d) 0.3mm and e) 1mm.

The quality of the wall section of both the 0.1mm and 0.15mm macrolayer samples is consistent with no visible porosity and a clear structure. The 0.2mm and 0.3mm samples show some deformation and porosity along the inner wall and infill interface with less definition in the wall structure. The 0.3mm cubes outer wall also shows some porosity and defects which do not appear in the 0.1mm and 0.15mm samples. All samples excluding the 1mm show a crossing pattern in the infill, with porosity present in all, however the percentage of this appears to increase as the macrolayer height increases.

Table 2 displays the quantified porosity within the cubes. It confirms the findings of the CTVox renderings with the porosity percentage increasing as the macrolayer height increases. This increase can also be attributed to the appearance of porosity and voids within the infill print path. This is not present in the 0.1mm sample and begins to appear in the 0.15mm sample, continuing to appear in increasing volume in the 0.2mm and 0.3mm macrolayer samples.

The 1mm sample presents double the quantified porosity percentage compared to the 0.3mm sample, and this quality difference is apparent in the CTVOx rendering. The sample does not show the “crossing/webbed” infill pattern seen in the other samples and instead displays large voids between the full length of the infill pattern. The inner wall and infill interface is not clearly defined as in the other samples and the wall shows a large concentration of voids, again different from all other samples where the wall quality is consistent. The deformation first seen in the 0.3mm sample to the external wall quality is greatly enhanced and a visible split within the wall has occurred, possibly caused by the decrease in print time not allowing adequate time for the layers to cool and bond.

*Table 2 - Porosity (%) values for all samples.*

<b>Sample</b>	<b>Porosity (%)</b>
0.1mm Macrolayer	0.62
0.15mm Macrolayer	1.79
0.2mm Macrolayer	3.04
0.3mm Macrolayer	5.06
1mm Macrolayer	10.70

### 3.3 Structural Assessment

#### 3.3.1 Mechanical properties

Figure 6 shows the stress strain curves for the samples across all profiles. To allow for IR monitoring, one sample in each set of 3 was tested without the digital extensometer. All samples perform in a brittle manner however there is a significant difference in the performance of the 1mm macrolayer samples compared to the 0.1-0.3mm samples, with a 2x increase in strain but a 40% decrease in ultimate tensile strength (UTS).

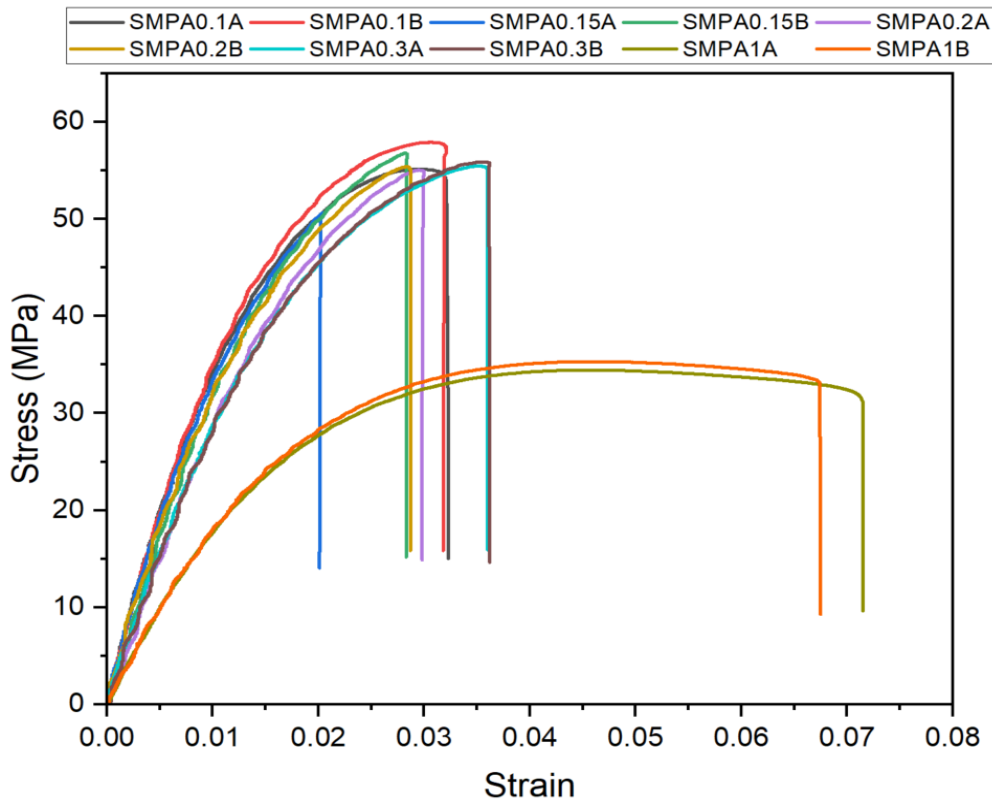


Figure 6 - Stress Strain curve for all samples.

Figure 7 shows a comparison of the average UTS and Young's modulus (E) across the sets of 3 samples. The samples were also compared to the data sheet values for Smooth PA provided by Anisoprint [14], UTS of  $71.63 \pm 1.67$  and Young's modulus of  $3304.39 \pm 145$ . When comparing UTS, the 0.1mm recorded the highest on average, but there was not a significant change between the 0.1-0.3mm samples, when compared to the increase in print time required. The Young's modulus of the samples displayed a trend of increasing as the macrolayer height decreased and the print time increased.

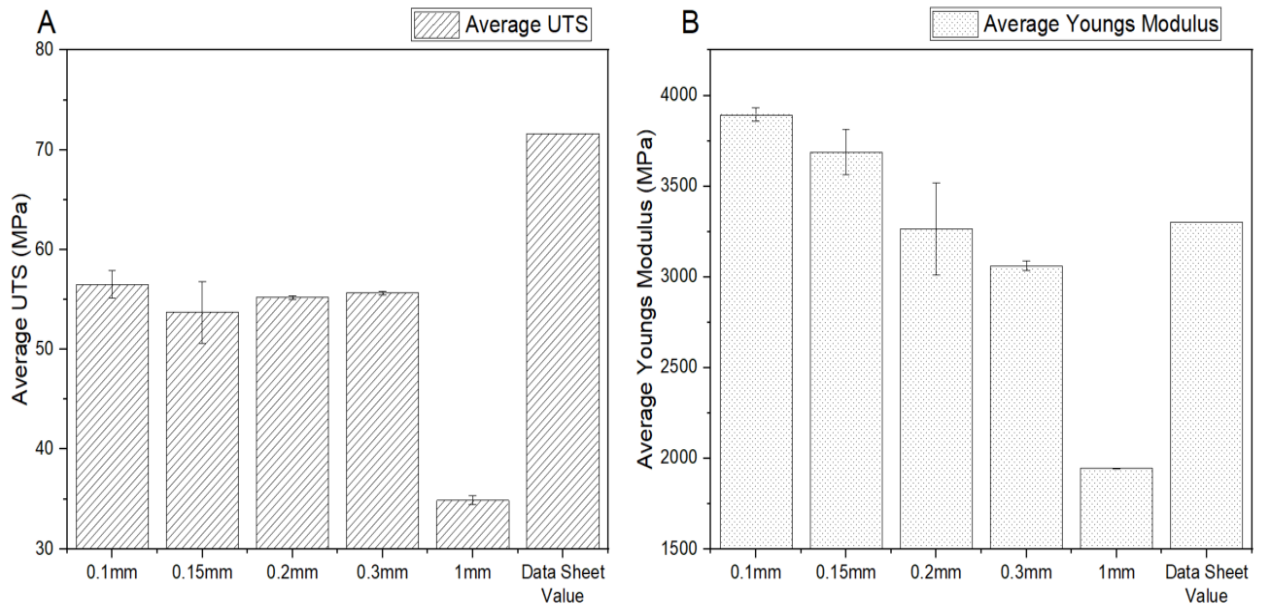


Figure 7 - Comparison of average a) Ultimate tensile strength and b) Young's modulus of all samples.

### 3.3.2 IR Monitoring

Figure 8 displays IR thermographs taken during the tensile testing of the samples. Utilising IR during the testing allows for the identification of other stress concentrators within the sample which did not lead to the full sample failure. Within the 0.15mm and 0.2mm samples (Figure 8b&c), secondary hotspots are visible separately from the beak locations. All the break locations and other hotspots excluding the 0.1mm and 1mm samples occur close to the radial sections of the samples and outside of the gauge length. This is a clear indication that these locations are stress concentrators and could be more prone to defects due to the nature of the printing process, as the print head moves freely and not in a coordinate direction. The 1mm sample (Figure 8e) shows hotspots throughout the sample once broken, indicating multiple high stress areas and defect locations.

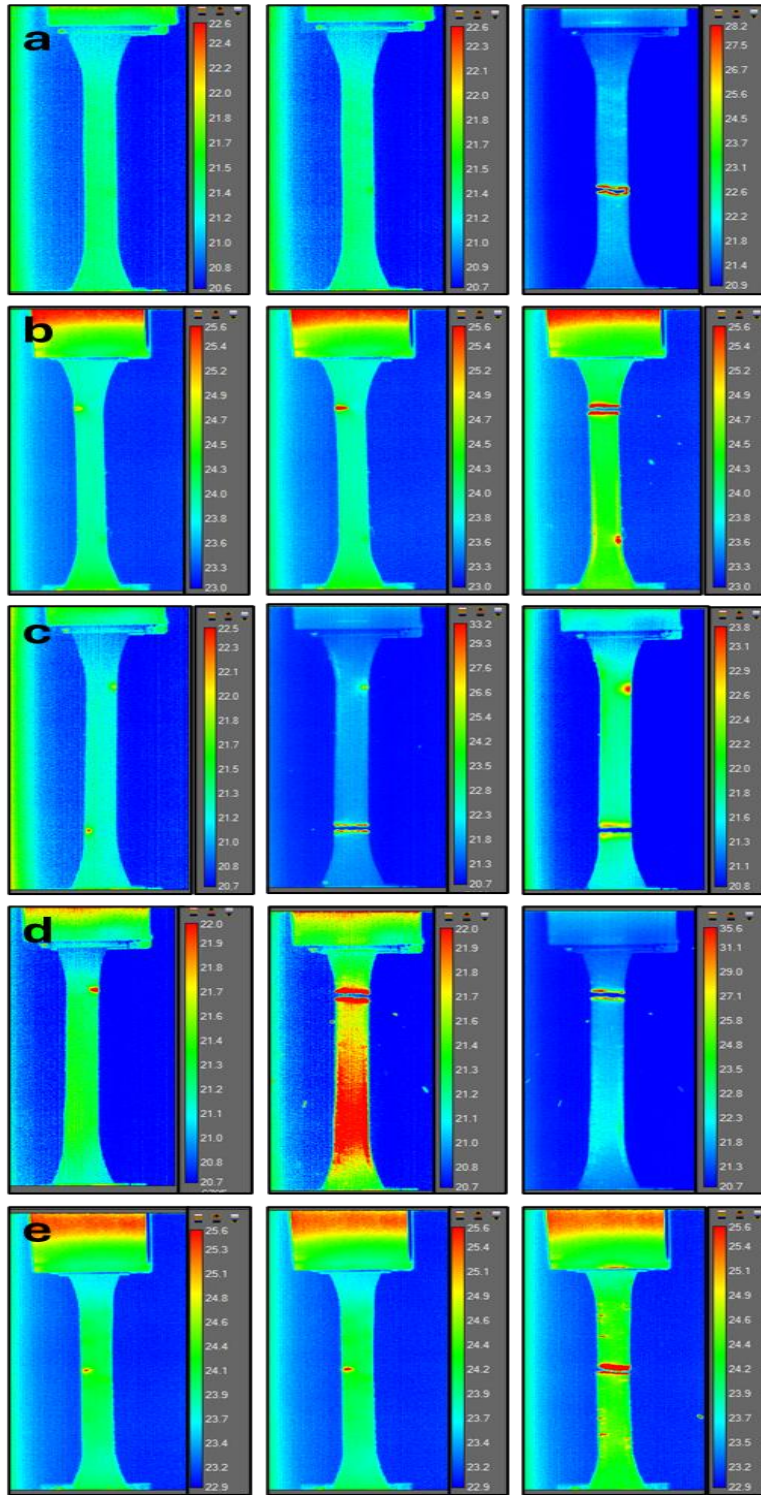


Figure 8 - IR thermographs during mechanical testing, a) 0.1mm, b) 0.15mm, c) 0.2mm, d) 0.3mm and e) 1mm.

#### 4. CONCLUSION

In this paper, a combination method of acoustic emission (AE) and infrared thermography (IR) alongside micro-computed tomography has been developed for the detection and monitoring of defects in additively manufactured short fibre-reinforced polymer matrix composites. The findings of the in-line monitoring were benchmarked against the offline assessment to determine efficacy. Multiple print setting profiles were compared to find a correlation between print time, print parameters and print quality. Structural assessment was also performed alongside IR monitoring to aid in the detection of stress concentrations and the presence of defects.

It was concluded that the combined methodology of in-line monitoring can detect abnormalities in the printing process and detect indicators of defects. This includes uneven material deposition, uneven thermal distribution and presence of porosity due to poor intra-layer fusion. The findings were benchmarked against the offline assessment which allowed for visualisation and quantification of the internal porosity. Compared to current methods of detecting defects in these materials, it supplies a non-destructive methodology which is backed up by the offline assessment findings.

A clear trend was discovered between the printing parameters, porosity and the mechanical properties of the samples, as the macrolayer height increases, the percentage of porosity increased, and the Young's modulus decreased.

The findings of this new combined methodology benchmarked against the Micro-CT requires further study and testing however the methodology can be used to determine abnormalities in the printing process which led to the formation of defects.

#### ACKNOWLEDGEMENTS

For the purpose of open access, the author has applied a Creative Commons Attribution (CC BY) licence to any Author Accepted Manuscript version arising from this submission.

This research was funded by the Sheffield Hallam University Graduate Teaching Assistant Scheme.

#### References

- [1] W. Gao, Y. Zhang, D. Ramanujan, K. Ramani, Y. Chen, C. B. Williams, C. C. L. Wang, Y. C. Shin, S. Zhang and P. D. Zavattieri, "The status, challenges, and future of additive manufacturing in engineering," *Computer Aided Design*, vol. 69, pp. 65-89, December 2015.
- [2] C. K. Chua, K. F. Leong and C. S. Lim, *Rapid prototyping: Principles and Application*, 3rd ed., World Scientific, 2010.
- [3] BSI Standards Publication, "Additive Manufacturing - General Principles - Terminology (BS EN ISO/ASTM 52900:2017)," BSI Standards Limited, 2017.
- [4] J. Li, Y. Durandet, X. Huang, G. Sun and D. Ruan, "Additively manufactured fiber-reinforced composites: a review of mechanical behaviour and opportunities," *Journal of Materials Science & Technology*, 2022.

- [5] S. Hisham, S. F. Khan and K. Kamarudin, "QUALITY MONITORING FOR FUSED FILAMENT FABRICATION PRODUCT: A REVIEW," *International journal of research and analytical reviews*, vol. IX, no. 2, April 2022.
- [6] D. Frunzaverde, V. Cojocaru, N. Bacescu, C.-R. Ciubotariu, C.-O. Miclosina, R. R. Turiac and G. Marginean, "The Influence of the Layer Height and the Filament Color on the Dimensional Accuracy and the Tensile Strength of FDM-Printed PLA Specimens," *Polymers*, vol. 15, 2023.
- [7] R. Jain, S. Nauriyal, V. Gupta and K. S. Khas, "Effects of Process Parameters on Surface Roughness, Dimensional Accuracy and Printing Time in 3D Printing," in *Advances in Production and Industrial Engineering, Select Proceedings of ICETMIE 2019*, 2020.
- [8] J. Butt, R. Bhaskar and V. Mohaghegh, "Analysing the effects of layer heights and line widths on FFF-printed thermoplastics," *The International Journal of Advanced Manufacturing Technology*, vol. 121, pp. 7383-7411, 2022.
- [9] T. Smith, J. Failla, J. Lindahl, S. Kim, A. A. Hassen, C. Duty, P. Joshi, C. Stevens and V. Kunc, "STRUCTURAL HEALTH MONITORING OF 3D PRINTED STRUCTURES," in *Solid Freeform Fabrication 2018: Proceedings of the 29th Annual International Solid Freeform Fabrication Symposium – An Additive Manufacturing Conference Reviewed Paper*, 2018.
- [10] E. Ferraris, J. Zhang and B. Van Hooreweder, "Thermography based in-process monitoring of Fused Filament Fabrication of polymeric parts," *CIRP Annals - Manufacturing Technology*, pp. 213-216, 2019.
- [11] A. Oleff, B. Küster, M. Stonis and L. Overmeyer, "Process monitoring for material extrusion additive manufacturing: a state-of-the-art review," *Progress in Additive Manufacturing*, pp. 705-730, 2021.
- [12] J. Soete, B. Badoux, Y. Swolfs, L. Gorbatikh and M. Wevers, "Defect detection in 3D printed carbon fibre composites using X-ray Computed Tomography," in *9th Conference on Industrial Computed Tomography*, Padova, 2019.
- [13] British Standards Institution, "Part 4: Test conditions for isotropic and orthotropic fibre-reinforced plastic composites," in *Plastics — Determination of tensile properties*, 2023.
- [14] Anisoprint, "Smooth PA Technical Data Sheet," August 2020.
- [15] FLIR, "FLIRX6000sc Series High-Speed MWIR Performance Camera," 2016. [Online]. Available: [http://www.flirmedia.com/MMC/THG/Brochures/RND\\_088/RND\\_088\\_US.pdf](http://www.flirmedia.com/MMC/THG/Brochures/RND_088/RND_088_US.pdf). [Accessed 14 October 2024].
- [16] MISTRAS - Physical Acoustics Corporation, "WD Sensor," 2011. [Online]. Available: [https://www.physicalacoustics.com/content/literature/sensors/Model\\_WD.pdf](https://www.physicalacoustics.com/content/literature/sensors/Model_WD.pdf). [Accessed 17 February 2023].
- [17] Bruker, "SkyScan1272 User Manual," 2018.